Hierarchical Control in Islanded DC Microgrids with Flexible Structures

Pulkit Nahata*, Alessio La Bella*, Riccardo Scattolini, Giancarlo Ferrari-Trecate

***Abstract*—A comprehensive hierarchical control architecture for islanded DC microgrids (DCmG) is proposed, achieving a well scheduled and balanced utilization of various resources. Unlike previous contributions, we discuss a top-to-bottom control scheme guaranteeing voltage stability and allowing for generic topologies. Our supervisory control layer comprises a secondary and a tertiary layer and it rests on top of a primary voltage layer. The tertiary layer is governed by an Energy Management System (EMS), which generates optimal power references and decision variables for generation units by solving an MPC problem at every sampling instant. In particular, the generated decision variables take decisions on turning ON/OFF dispatchable generators, and operation modes of PV generators and batteries. The secondary layer receives power references from the EMS and translates them into appropriate voltage references for the primary layer by solving an optimization problem. We show that a simplified version of the secondary optimization problem is guaranteed to be always feasible. Moreover, since the voltages can only be enforced at the generator nodes, we provide a novel condition to guarantee the uniqueness of the solution for load voltages and power injection of the generation units. This uniqueness condition can be verified at each load node by utilizing local load parameters, and does not require any information about microgrid topology. Notwithstanding that EMS commands can alter the topology of the DCmG, switching on or off some generation nodes, the overall voltage stability is maintained by decentralized primary controllers. The functioning of the proposed architecture is validated via simulations on a modified 16-bus DC system [1].**

I. Introduction

Microgrids (mGs) are small-scale electric networks consisting of Distributed Generation Units (DGUs) interfaced with power-electronic converters and of different loads. Apart from their manifold advantages like integration of renewable energy sources, enhanced power quality, reduced transmission losses and capability to operate in grid-connected and islanded modes, mGs are compatible with both AC and DC operating standards [2]–[4]. In particular, DC microgrids (DCmGs), have gained traction in recent times. Their rising popularity can be attributed to the development of efficient converters, natural interfaces with renewable energy sources (for instance PV modules), batteries, and many electronic loads (various appliances, LEDs, electric vehicles, computers etc), inherently DC in nature [5], [6].

* indicates equal contribution. Pulkit Nahata and Giancarlo Ferrari-Trecate are with the Automatic Control Laboratory, École Polytechnique Fédérale de Lausanne, Lausanne, Switzerland. Alessio La Bella and Riccardo Scattolini are with the Department of Electronics, Information and Bioengineering, Politecnico di Milano, Milano, Italy. Email addresses: {pulkit.nahata, giancarlo.ferraritrecate}@epfl.ch, {alessio.labella,riccardo.scattolini}@polimi.it

This work has received support from the Swiss National Science Foundation under the COFLEX project (grant number 200021_169906) and the Research Fund for the Italian Electrical System in compliance with the Decree of Minister of Economic Development April 16, 2018.

A stable and economic operation of an islanded DC microgrid (DCmG) is a multi-objective problem and necessitates to properly regulate the internal voltages and to efficiently coordinate DGU operations while taking into consideration the non-deterministic absorption/production of loads and renewable energy sources. To this aim, a hierarchical architecture spanning different control stages, time scales, and physical layers is often employed [5]–[8].

Generally, a primary control layer, acting at the component level, is responsible for voltage stability, which is crucial in islanded DCmGs interfaced with nonlinear loads [9]. Many research studies have aimed at designing decentralized stabilizing primary controllers, implemented at each DGU with a view to tracking suitable voltage references. For this purpose, different techniques such as droop control [3], [5], plug-and-play [9], [10] and sliding-mode control [11] have been explored. Primary controllers nonetheless are blind voltage emulators and are incapable of incorporating various operational and economic constraints necessary for ensuring the continuous and proper functioning of the islanded DCmG. High-level supervisory control architectures are, therefore, necessary to coordinate the voltage references provided to the primary layers. Consensus-based controllers assigning appropriate voltage references to guarantee proportional load sharing and voltage balancing are discussed in [12], [13]. Despite their distributed structure, these controllers assume load satisfiability and unsaturated inputs at all times. Supervising control strategies considering saturated inputs for primary voltage controllers are proposed in [14], however neglecting DGUs capability limits and dynamics. These limitations can be overcome by designing an energy management system (EMS), which can meet specified power and energy management strategies while respecting generation constraints and other economic objectives like optimal power dispatch, load sharing, and battery management. Flowchart-based EMS encompassing multiple case scenarios are discussed in [15], [16] whereas the use of optimization methods and predictive algorithms to design an EMS is investigated in [8], [17].

In general, EMS, notably when based on complex optimization algorithms such as stochastic or mixed-integer techniques, utilize power balance equations to provide optimal power set-points to the DGU units [18]–[21]. When the primary layer is voltage controlled, these EMS cannot be directly implemented in DCmG as the optimal power references must somehow be translated into suitable voltage set-points. Such a translation is not straightforward for mGs with meshed topologies and, effectively, requires the solution of power-flow equations. Moreover, considering that the voltages can solely be enforced by the DGUs, a unique voltage equilibrium may fail to exist at

the load buses in the presence of nonlinear loads (for example constant power loads) [22].

A. Main Contributions

The mentioned issues motivated the design of a comprehensive three-layered hierarchical control architecture for the overall operation and control of an islanded DCmG with arbitrary topologies. A schematic of the proposed architecture is depicted in Figure 2, and it is structured as follows.

- *Tertiary layer*: An EMS sits at the upper level, designed with a Model Predictive Control (MPC) strategy to define the optimal power references for DGU units, and their operating modes, based on system constraints and objectives.
- *Secondary layer*: A novel secondary control scheme, acting as an interface between the primary and the tertiary layer, converts the power signals provided by the tertiary level into voltage references for them to be tracked by the primary voltage regulators.
- *Primary layer*: The low-level layer is constituted by the decentralized voltage controllers, assumed to be present at all DGUs.

Different from [15], [16], [21], we study an islanded DCmG with a generic topology in the presence ZIP (constant impedance, constant current, and constant power) loads. In particular, we consider DGUs interfaced with nonrenewable dispatchable resources, batteries, and PV modules. In order to leverage the advances in grid-stabilizing decentralized primary voltage control, we assume that all DGUs are equipped with primary voltage regulators. We note that the control scheme can also incorporate scenarios where some DGUs are current-controlled [23], without compromising its validity. The structure and design of primary voltage controllers along with stability certificates and proofs are skipped in this work. A detailed analysis can be found in [9], [24], which show control design based on the Plug-n-Play paradigm, allowing DGUs to effortlessly enter/leave the DCmG without spoiling overall voltage stability.

The EMS generates optimal power references and the operating modes of DGUs by solving an MPC mixed-integer problem at every sampling instant while taking into account forecasts and system parameters. The considered integer variables serve to turn ON/OFF dispatchable DGUs, switch the PV DGUs between Maximum Power Point Tracking (MPPT) and power curtailment modes, and control the operation mode of batteries by either charging or discharging them. In spite of a change in topology that may take place due to EMS commands, the collective voltage stability of the DCmG network is ensured by decentralized Plug-n-Play primary controllers.

The secondary layer utilizes the optimal power references transmitted by the EMS and translates them into appropriate voltage references for the primary controllers. This power-voltage conversion at the secondary layer is facilitated by an optimization problem, which is based on the power-flow equations and takes into account the converter and network losses. We prove that this optimization problem, although nonlinear and non-convex, is always feasible if nodal voltages and power injections are not bounded. The existence of a solution to the power-flow equations, necessary for the feasibility of the optimization problem, has been addressed in [25], [26] with fixed DGUs voltages. Nevertheless, the provided conditions for existence can not be used directly as the DGU voltage references are here free optimization variables and not known *a priori*. Furthermore, as a complement, we also state a necessary condition for the solvability of the stated optimization problem.

We highlight that the voltages can only be enforced at the DGUs nodes and therefore, the uniqueness of voltages appearing at the load nodes is necessary for attaining the predefined operational objectives. Indeed, if the load voltages are different from the ones anticipated by the secondary layer, permissible voltage limits may be violated and DGUs may fail to track the optimal power set-points provided by the EMS. In this respect, we provide a novel condition for the uniqueness of load voltages and DGU power injections. The uniqueness of voltages has also been addressed in [25], where the deduced condition depends on the generator voltages and the topological parameters of the overall network. Here, we provide a novel and simpler condition that depends only on local load parameters and can be easily taken into account while designing the DCmG network. Finally, the robustness of the proposed control scheme in the presence of inaccurate generation and load forecasts is tested on a modified 16-bus feeder [1].

Preliminary results concerning this work have been reported in [27] where (i) design of an EMS was deferred to future work, (ii) interface between secondary and tertiary layers was not discussed, (ii) no distinction was made on the type of DGU and their dynamics was not modelled, and (iv) detailed proofs of main theorems and propositions were skipped. Furthermore, this article demonstrates a coordinated operation of multiple control layers on a 16-node DCmG.

The structure of DCmG along with proposed hierarchical control scheme is described in Section II. The EMS-based tertiary layer and its interaction with the secondary control layer is detailed in Section III. The in-depth functioning of secondary layer and related derivations are presented in Section IV. Simulations validating theoretical results are provided in Section V, testing the proposed control architecture on a modified 16-bus DC feeder, described in [1]. Finally, conclusions are drawn in Section VI.

B. Preliminaries and notation

Sets, vectors, and functions: We let $\mathbb{R}$ (resp. $\mathbb{R}_{>0}$) denote the set of real (resp. strictly positive real) numbers. Given $x \in \mathbb{R}^n$, $[x] \in \mathbb{R}^{n\times n}$ is the associated diagonal matrix with x on the diagonal. The inequality $x \leq y$ for vectors $x, y \in \mathbb{R}^n$ is component-wise, that is, $x_i \leq y_i, \ \ \forall i \in 1, ..., n$. For a finite set $\mathcal{V}$, let $|\mathcal{V}|$ denote its cardinality. Given a matrix $A \in \mathbb{R}^{n\times m}$, $(A)_i$ denotes the i^{th} row. The notation $A \succ 0$, $A \succeq 0$, $A > 0$, and $A \geq 0$ represents a positive definite, positive semidefinite, positive, and nonnegative matrix, respectively. Throughout, $\mathbf{1}_n$ and $\mathbf{0}_n$ are the n-dimensional vectors of unit and zero entries, and $\mathbf{0}$ is a matrix of all zeros of appropriate dimensions. Given

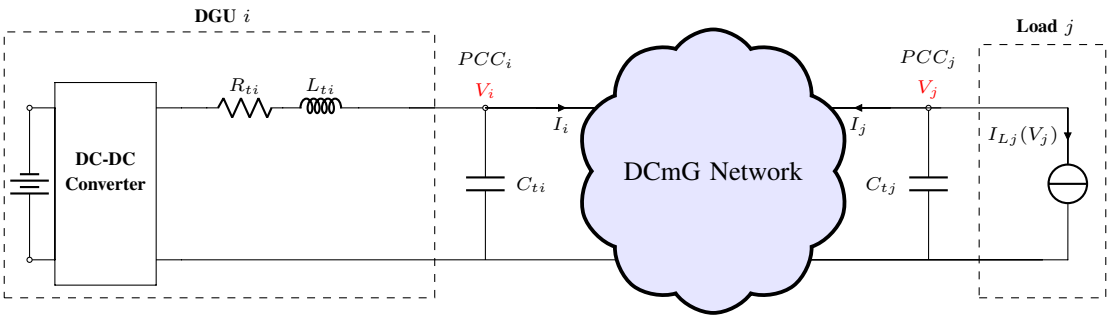

Fig. 1: Representative diagram of the DCmG network with DGUs and loads.

a weighted directed graph $\mathcal{G}(\mathcal{V}, \mathcal{E})$, with $\mathcal{V}$ the set of nodes and $\mathcal{E}$ the set of edges, its Laplacian matrix $L \in \mathbb{R}^{|\mathcal{V}|\times|\mathcal{V}|}$ is defined as

$$L = A\,\mathbf{1}_{|\mathcal{V}|} - A,$$

where A is the adjacency matrix of $\mathcal{G}$ collecting edges weights and is defined as

$$a_{ij} = \begin{cases} w_{ij} & \text{if } (i,j) \in \mathcal{E} \\ 0 & \text{otherwise} \end{cases}.$$

II. DC MICROGRID STRUCTURE AND HIERARCHICAL CONTROL SCHEME

In this section, we describe the DCmG structure and provide an outline of the hierarchical control structure used to ensure optimal, safe, and uninterrupted operation of the network.

Structure of the DC microgrid: The electric interconnections in an DCmG, comprising multiple DGUs connected to each other via power lines, are modeled as an undirected connected graph $m\mathcal{G} = (\mathcal{V}, \mathcal{E})$. $\mathcal{V}$ is partitioned into two sets: $\mathcal{G}$ is the set of DGUs and $\mathcal{L}$ is the set of loads. The edges represent the interconnecting lines of the mG. As shown in Figure 1, each DGU and load is interfaced with the DCmG through a point of common coupling (PCC).

Distributed generation units (DGUs): The DGUs comprise a DC voltage source, a DC-DC converter, and a series RLC filter. Additionally, depending upon the type of DC voltage source, we define $\mathcal{G}_D$ as the set of dispatchable DGUs, $\mathcal{G}_B$ as the set of DGUs interfaced with batteries, and $\mathcal{G}_P$ as the set of DGUs connected to PV panels, where $\mathcal{G}_D \cup \mathcal{G}_B \cup \mathcal{G}_P = \mathcal{G}$.

Load model: Depending upon the type of load, the functional dependence on the PCC voltage changes and the term $I_{Lj}(V_j)$ takes different expressions. Prototypical load models that are of interest include the following:

1) constant-current loads: $I_{LI,j} = \bar{I}_{L,j}$,
2) constant-impedance loads: $I_{LZ,j}(V_j) = Y_{L,j}V_j$, where $Y_{L,j} = 1/R_{L,j} > 0$ is the conductance of the j^{th} load, and
3) constant-power loads:

$$I_{LP,j}(V_j) = V_j^{-1}\bar{P}_{L,j}, \tag{1}$$

where $\bar{P}_{L,j} > 0$ is the power demand of the load j.

To refer to the three load cases above, the abbreviations "I", "Z", and "P" are often used [28]. The analysis presented in this article will focus on the general case of a parallel combination of the three loads, thus on the case of "ZIP" loads, which are modeled as

$$I_{L,j}(V_j) = \bar{I}_{L,j} + Y_{L,j}V_j + V_j^{-1}\bar{P}_{L,j}. \tag{2}$$

The net power absorbed by the j^{th} load is given as

$$P_{L,j}(V_j) = \bar{I}_{L,j}V_j + Y_{L,j}V_j^2 + \bar{P}_{L,j}. \tag{3}$$

A. Hierarchical control in DC microgrids

In this work, we propose the hierarchical control architecture depicted in Figure 2. The controller is split into three distinct layers *viz.* primary, secondary, and tertiary. The secondary and tertiary layers together form the supervisory control layer of the DCmG network.

All DGUs are equipped with local voltage regulators (not shown in Figure 1) forming the *primary control layer*. The main objective of these controllers is to ensure that the voltage at each DGU's PCC tracks a reference voltage V_i^* provided by the *supervisory control layer*.

Assumption II.1. ***(Stability under primary voltage control).*** *It is assumed that the primary controllers, under constant voltage*

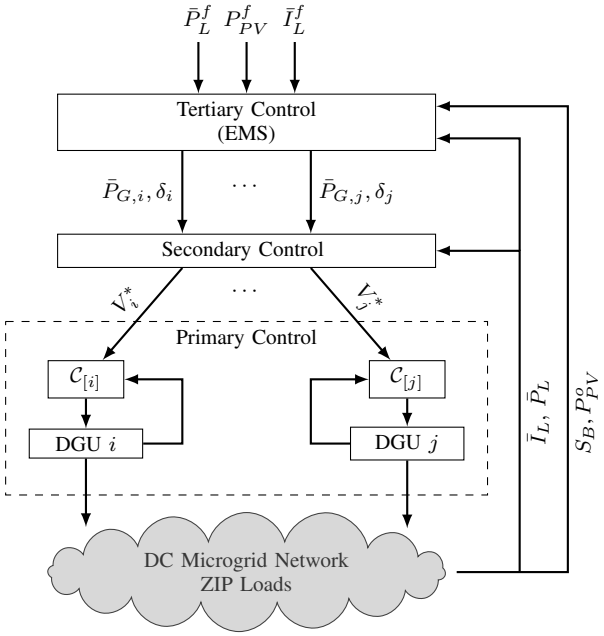

Fig. 2: Hierarchical control scheme for DC microgrids.

reference $V_i^*, i \in \mathcal{G}$, achieve offset-free voltage tracking and guarantee the stability of the entire DCmG network. The reader is deferred to [6], [9], [24] and the references therein for further details concerning design of stabilizing primary controllers.

An EMS sits at the tertiary level, and utilizes the forecasts of PV generation P_{PV}^f, and loads' power and current absorption terms $\bar{P}_L^f$, $\bar{I}_L^f$. At each time step, it measures the nominal PV generation P_{PV}^o, the state of charge (SOC) of batteries S_B and the actual power and current absorption of ZIP loads $\bar{P}_L, \bar{I}_L$. Solving an MPC optimization problem, the EMS generates optimal power references $\bar{P}_{G,i}, i \in \mathcal{G}$, for the DGUs. In addition, it produces decision variables $\delta_i \in \{0,1\}, i \in \mathcal{G}$, which can either turn on/off DGUs or change their operation mode. Since the primary layer operates only with voltage references, the secondary control layer translates the power references into appropriate voltage references V^*. The detailed structure and functioning of the secondary and tertiary control layers are discussed in Sections IV and III, respectively.

We highlight that different layers work at different time scales. In a typical scenario, the primary controllers operates in a range varying from 10^{-6} to 10^{-3} s, the secondary layer ranges from 100 to 300 s, and the tertiary layer ranges from 5 to 15 mins. At each high level sampling time, the controller provides a reference to its corresponding lower layer.

III. Tertiary control layer: the EMS

This section details the functioning of the MPC-based EMS, sitting at the top of the proposed hierarchical structure. The forecasts, parameters, and decision variables are described in Table I. As a convention, all the power values are defined to be positive if delivered from a DGU. Moreover, the upper and lower bounds of each variable are denoted with superscripts max and min, respectively.

A. MPC-based EMS for islanded DCmGs

The MPC-based EMS controller is responsible for energy management and coordination of resources in the islanded DCmG. The core of this controller is a receding horizon optimization problem, which enables load satisfiability, optimal scheduling of dispatchable and storage DGUs, and maximum possible utilization of PV DGUs.

The EMS is formulated as a mixed integer optimization problem, executed at the generic time instant k, with a finite prediction horizon $[k, \ldots, k+N]$, where N indicates the number of prediction steps. In the following discussion, the index i is used to define variables and constraints spanning all prediction horizon, i.e. $i \in [0, \ldots, N]$. The MPC-based EMS, at each time step, defines an optimal plan is formulated on power dispatch, storage schedule, and operational modes of the units for the whole prediction horizon. However, only the first sample of the input sequence is implemented and subsequently the horizon is shifted. At the next sampling time, using updated information on forecasts and mG initial condition, a new optimization problem is solved. Next, we describe the EMS in detail.

TABLE I: Optimization variables and system parameters for the EMS

Symbol	Description
P_{DH}, P_{CH}	Charging and discharging power of the battery [kW]
P_B	Power output of battery DGUs [kW]
P_D	Power output of dispatchable DGUs [kW]
P_{PV}	Power output of PV DGUs [kW]
P_{PV}^o	Nominal power production of PV DGUs [kW]
P_{PV}^f	Power production forecast of PV DGUs [kW]
P_L^o	Nominal total power absorption for ZIP loads [kW]
$\bar{I}_L^f$	Current absorption forecast for I load [kVar]
$\bar{P}_L^f$	Power absorption forecast for P load [kW]
S_B	State of charge (SOC) of battery
S_B^o	Nominal SOC of battery
η_{CH}, η_{DH}	Charging and discharging efficiency of battery
C_B	MG battery capacity [kWh]
V^o	Nominal network voltage [V]
δ_B	Operation mode of battery DGU [boolean]
δ_D	Operation mode of dispatachable DGU [boolean]
δ_{PV}	Operation mode of PV DGU [boolean]
V	Nodal voltage magnitude [V]
I	Nodal current magnitude [A]

1) *DGUs*: Based upon the type of voltage source, the DGUs are characterized differently for the EMS.
   a) Storage DGUs: For these DGUs, a battery serves as the voltage source. The SOC dynamics of a battery $b \in \mathcal{G}_B$, considering both the charging and discharging efficiencies, are given as

$$S_{B,b}(k+1+i) = S_{B,b}(k+i) - \frac{\tau}{C_{B,b}}\left(\frac{1}{\eta_{DH,b}} P_{DH,b}(k+i) + \eta_{CH,b} P_{CH,b}(k+i)\right), \tag{4}$$

   with battery power output

$$P_{B,b}(k+i) = P_{DH,b}(k+i) - P_{CH,b}(k+i). \tag{5}$$

   Since battery DGUs can operate either in charging or discharging mode, the following constraints are stated

$$0 \leq P_{DH,b}(k+i) \leq P_{B,b}^{max}(k+i)\,\delta_{B,b}(k+i), \tag{6}$$

$$0 \leq P_{CH,b}(k+i) \leq -P_{B,b}^{min}(k+i)\,(1-\delta_{B,b}(k+i)), \tag{7}$$

   where $\delta_{B,i} = 1$ indicates discharging mode while $\delta_{B,i} = 0$ represents the charging mode. In order to ensure longevity of batteries, the SOC is constrained between minimum and maximum bounds

$$S_{B,b}^{min} \leq S_{B,b}(k+i) \leq S_{B,b}^{max}. \tag{8}$$

   The constraints (4)-(8) must be stated $\forall i \in [0, \ldots, N-1]$. To avoid complete charging or discharging of batteries, not ideal for guaranteeing voltage stability and load satisfiability for all possible contingencies, a terminal constraint on the SOC is imposed

$$S_{B,b}(k+N) = S_{B,b}^o + \Delta S_{B,b}\,, \tag{9}$$

where $S^o_{B,b}$ is the nominal SOC of battery $b \in \mathcal{G}_B$, while $\Delta S_{B,b}$ is a slack variable introduced to ensure feasibility.

b) Dispatchable DGUs: These DGUs are interfaced with a nonrenewable energy resource, and these can be switched on, or off, based on the DCmG necessity. The operational mode is governed by the variable $\delta_{D,d}, d \in \mathcal{D}_\mathcal{D}$, with values 1 and 0 indicating on and off states, respectively. The power produced by the dispatchable DGU lies within a range defined by lower and upper bounds

$$\begin{aligned} \delta_{D,d}(k+i)\, P^{min}_{D,j} \;&\leq\; P_{D,d}(k+i) \\ P_{D,d}(k+i) \;&\leq\; P^{max}_{D,d}\, \delta_{D,d}(k+i), \quad d \in \mathcal{G}_D, \end{aligned} \tag{10}$$

defined $\forall i \in [0, \ldots, N-1]$.

c) PV DGUs: We note that the p^{th} DGU, $p \in \mathcal{G}_P$, has two distinct modes of operation: power curtailment mode and MPPT. In power curtailment mode, the DGU's power is curtailed in order to respect the operational limits whereas the maximum possible power is injected into the grid when PV DGUs are operated in MPPT mode. To preserve internal power balance during periods of peak PV generation, power curtailment is sometimes unavoidable. Since, at a given time instant, the EMS utilizes both the actual nominal PV generation and the forecast for future time instants, the PV power output expressed as

$$P_{PV,p}(k) = P^o_{PV,p}(k) \Delta P_{PV,p}(k),\ p \in \mathcal{G}_P, \tag{11}$$

$$P_{PV,p}(k+i) = P^f_{PV,p}(k+i) - \Delta P_{PV,p}(k+i), \tag{12}$$

$\forall i \in [1, \ldots, N-1]$, where $\Delta P_{PV,p}$ expresses the amount of curtailed power. The curtailed power cannot be arbitrary and fulfills the constraints

$$\Delta P_{PV,p}(k) \geq (1 - \delta_{PV,p}(k))\, \epsilon, \tag{13}$$

$$\Delta P_{PV,p}(k) \leq (1 - \delta_{PV,p}(k))\, P^o_{PV,p}(k), \tag{14}$$

$$\Delta P_{PV,p}(k+i) \geq (1 - \delta_{PV,p}(k+i))\epsilon, \tag{15}$$

$$\Delta P_{PV,p}(k+i) \leq (1 - \delta_{PV,p}(k+i))\, P^f_{PV,p}(k+i), \tag{16}$$

$\forall i \in [1, \ldots, N-1]$, where $\epsilon > 0$ is a sufficiently small number and $\delta_{PV,p}$ is a decision variable. The rationale behind constraints (13)-(16) is not only to limit power curtailment but also to enable just one of the operation modes. Clearly, if $\delta_{PV,p} = 1$, $\Delta P_{PV,p}$ is forced to zero meaning that the MPPT mode is activated, whereas if $\delta_{PV,p} = 0$, the curtailed power must be strictly greater than zero and lower than the effective PV power production. For more details on logic and mixed-integer constraints, the reader is referred to [29].

2) *Loads:* The nominal power absorption of the l^{th} ZIP load, $l \in \mathcal{L}$, is computed at nominal voltage by utilizing the current state of the system for the first time step

$$P^o_{L,l}(k) = \bar{I}_{L,l}(k) V^o + Y_{L,l} V^{o2} + \bar{P}_{L,l}(k),\ l \in \mathcal{L}, \tag{17}$$

while forecasts are used for future time instants $i \in [1, \ldots, N-1]$ as

$$P^o_{L,l}(k+i) = \bar{I}^f_{L,l}(k+i) V^o + Y_{L,l} V^{o2} + \bar{P}^f_{L,l}(k+i). \tag{18}$$

It is worth noticing that $P^o_{L,l}$ is just an estimate, as net power absorption of ZIP loads depends on the actual DCmG voltages, as reported in (3).

3) *Power balance:* In an islanded DCmG, the internal power balance must be maintained. Hence, the following constraint is expressed

$$\begin{aligned} &\sum_{b \in \mathcal{D}_\mathcal{B}} P_{B,b}(k+i) + \sum_{d \in \mathcal{D}_\mathcal{D}} P_{D,d}(k+i) \\ &\quad + \sum_{p \in \mathcal{D}_\mathcal{P}} P_{PV,p}(k+i) + \sum_{l \in \mathcal{L}} P^o_{L,l}(k+i) = 0, \end{aligned} \tag{19}$$

which is stated $\forall i \in [0, \ldots, N-1]$. We highlight that the converter and network losses are neglected at the EMS level.

4) *Cost function:* The aim is to minimize the cost of satisfying the electrical loads, hence the cost function is

$$\begin{aligned} J(k) = \;& \\ &\sum_{b \in \mathcal{D}_\mathcal{B}} (\Delta S_{B,b})^2 w_{S,b} + \sum_{i=0}^{N-1} \sum_{b \in \mathcal{D}_\mathcal{B}} (P_{B,b}(k+i))^2 w_{B,b} \\ &+ \sum_{i=0}^{N-1} \sum_{d \in \mathcal{D}_\mathcal{D}} (P_{D,d}(k+i))^2 w_{D,d} \\ &+ \sum_{i=0}^{N-1} \sum_{p \in \mathcal{D}_\mathcal{P}} (\Delta P_{PV,p}(k+i))^2\, w_{PV,p} \\ &+ \underbrace{\sum_{i=0}^{N-1} \sum_{p \in \mathcal{D}_\mathcal{P}} (\delta_{PV,p}(k+i) - \delta_{PV,p}(k+i-1))^2 w \delta_{PV,p}}_{\alpha} \\ &+ \underbrace{\sum_{i=0}^{N-1} \sum_{b \in \mathcal{D}_\mathcal{B}} (\delta_{B,b}(k+i) - \delta_{B,b}(k+i-1))^2 w \delta_{B,b}}_{\beta} \\ &+ \underbrace{\sum_{i=0}^{N-1} \sum_{d \in \mathcal{D}_\mathcal{D}} (\delta_{D,d}(k+i) - \delta_{D,d}(k+i-1))^2 w \delta_{D,d}}_{\gamma}, \end{aligned} \tag{20}$$

where $w_S, w_{PV}, \ldots$ are positive weights. We intend on keeping batteries close to their nominal SOCs and using power curtailment as the last resort. Thus, the weights $w_{S,B}$ and w_{PV} are set to much higher values with respect to others, enabling $\Delta S_{B,b}$ and $\Delta P_{PV,p}$ to be nonzero only when necessary for preserving feasibility. The terms α, β and γ are included in the cost to avoid frequent changes in modes of operation of different DGUs.

At every EMS time instant, the following optimization is solved to obtain optimal power set points $\bar{P}_{B,i}, \bar{P}_{D,j}, \bar{P}_{PV,p}$ and decision variables $\delta_{B,i}, \delta_{D,j}, \delta_{PV,p}$.

$$J_{EMS}(k) = \min J(k) \tag{21a}$$

subject to

$$(4) - (19). \tag{21b}$$

B. Interaction between tertiary and secondary layers

The EMS produces power references as well as decision variables, both of which are passed down to the secondary control layer. The value of these decision variables essentially determines the topology of the DCmG network. This is due to the fact that dispatchable generator nodes can be connected/disconnected from the network based on the value of $\delta_{D,j}$. Moreover, based on the value of $\delta_{PV,p}$, the PV DGUs can either inject maximum power or undergo power curtailment. While injecting maximum power, the PV DGU is governed by standard MPPT algorithms and automatically alters its output voltage in order to inject maximum power. Thus, in this mode, the DGU operates as a P load injecting power. When the DGU experiences a power curtailment, it injects the requested power and operates as a voltage-controlled DGU.

As mentioned earlier, the EMS power references are not directly perceivable by the primary controllers. Thus, a power-to-voltage translation is performed by the secondary controller by utilizing topology-based power-flow equations (see Section IV). Therefore, at every EMS time instant, the secondary controller uses the decision variables to update the DCmG topology in order to accommodate the turning ON/OFF of dispatchable generators as well as operation mode of PV DGUs.

Remark III.1. ***(Connectivity of the DCmG network).*** *It is assumed that the turning ON/OFF of dispatchable DGUs does not impact the connectivity of the rest of the DCmG network. In other words, addition or removal of a dispatchable DGUs must not split the remainder of the network into two or more disjoint islanded mGs. In case, critical DGUs affecting the connectivity of graph are present in the network, one can restrict their operation modes by adding additional constraints to the EMS optimization problem (see Section V for an example).*

IV. Secondary control based on power-flow equations

The secondary control is designed to make DGUs track the power references provided by the EMS, now denoted as $\bar{P}_G$. We highlight that the decision variables communicated by the EMS at a given sampling instant define the topology of the network over the next EMS sampling period.

Remark IV.1. *The secondary layer, operating on a faster time scale in comparison to the EMS, utilizes a fixed DCmG topology over an EMS sampling period to perform power-voltage translation. The topology is updated when a new set of decision variables is received.*

To perform the power-to-voltage translation, such that proper references can be sent to primary controllers, we first start by deducing the equations linking power and voltage. The relation between power and voltage in an islanded DCmG is defined by the power-flow equations dependent on mG parameters and topology.

We let the undirected connected graph $m\tilde{\mathcal{G}} = (\tilde{\mathcal{V}}, \tilde{\mathcal{E}})$ define the topology of the DCmG for a specified EMS sampling period. The set $\tilde{\mathcal{V}}$ is partitioned into two sets: $\tilde{\mathcal{G}} = \{1, \ldots, n\}$ is the set of DGUs and $\tilde{\mathcal{L}} = \{n+1, \ldots, n+m\}$ is the set of loads. The set $\tilde{\mathcal{G}} = \tilde{\mathcal{G}}_D \cup \tilde{\mathcal{G}}_B \cup \tilde{\mathcal{G}}_P^G$, where $\tilde{\mathcal{G}}_D$ is the set of connected dispatchable DGUs, $\tilde{\mathcal{G}}_B$ is the set of batteries, and $\tilde{\mathcal{G}}_P^D$ is the set of voltage-controlled PV DGUs. In steady state, the inductances and capacitances can be neglected and the current-voltage relation is given by the identity $I = B\Gamma B^T V = YV$, where $B \in \mathbb{R}^{(n+m)\times|\mathcal{E}|}$ is the incidence matrix of $m\tilde{\mathcal{G}}$, I is the vector of PCC currents, V is the vector containing PCC voltages (see Figure 1), Γ is the diagonal matrix of line conductances, and $Y \in \mathbb{R}^{(n+m)\times(n+m)}$ is the network admittance matrix [30]. On partitioning the nodes into DGUs and loads, the relation can be rewritten as

$$\begin{aligned}\begin{bmatrix} I_G \\ I_L \end{bmatrix} &= \begin{bmatrix} B_G R^{-1} B_G^T & B_G R^{-1} B_G^T \\ B_L R^{-1} B_G^T & B_L R^{-1} B_G^T \end{bmatrix} \begin{bmatrix} V_G \\ V_L \end{bmatrix} \\ &:= \begin{bmatrix} Y_{GG} & Y_{GL} \\ Y_{LG} & Y_{LL} \end{bmatrix} \begin{bmatrix} V_G \\ V_L \end{bmatrix}\end{aligned}, \tag{22}$$

where $V_G = [V_1, \ldots, V_n]^T$, $V_L = [V_{n+1}, \ldots, V_{n+m}]^T$, $I_G = [I_1, \ldots, I_n]^T$, and $I_L = [I_{n+1}, \ldots, I_{n+m}]^T$. The subscripts G and L indicate the DGUs and loads, respectively. Throughout this work, the following assumption is made.

Assumption IV.1. *The PCC voltage V_i is strictly positive for all $i \in \mathcal{V}$.*

We remark that Assumption IV.1 is not a limitation, and rather reflects a common constraint in microgrid operation. Notice that, in Figure 1, one end of the load is connected to the PCC and the other to the ground, assumed be at zero potential by convention. Since the electric current flows from higher to lower potential, negative references and PCC voltages would reverse the role of loads and make them power generators. In order to ensure power balance in the network, this power would be absorbed by the generators. This, in effect, defeats the fundamental goal of the mG, that is, the satisfiability of the loads by virtue of the power generated by the DGUs. Furthermore, if $V_i \in \mathbb{R}^N$, then a zero-crossing for the voltages may take place. At zero voltage, the power consumed by the ZIP loads tends to infinity.

Based on the current directions depicted in Figure 1, it is evident that $I_{L,j}(V_j) = -I_j,\ j \in \mathcal{L}$. Using (2), one can simplify (22) as

$$I_G = Y_{GG} V_G + Y_{GL} V_L \tag{23a}$$

$$0 = Y_{LG} V_G + Y_{LL} V_L + Y_L V_L + \bar{I}_L + [V_L]^{-1} \bar{P}_L, \tag{23b}$$

where $Y_L \in \mathbb{R}^{m\times m}$ is the diagonal matrix of load admittances. The vectors $\bar{I}_L$ and $\bar{P}_L$ collect consumptions of I and P loads, respectively. Note that the power $P_{G,i}, i \in \tilde{\mathcal{G}}$ produced by an individual DGU is the sum of power injected into the network and the filter losses. Equivalently,

$$P_G = [V_G] I_G + [I_G] R_G I_G \tag{24}$$

where $R_G \in \mathbb{R}^{n\times n}$ is a diagonal matrix collecting filter resistances and I_G is the vector of DGU filter currents. On pre-multiplying (23a) with $[V_G]$, and by using (24), one can rewrite (23) as

$$\begin{aligned} f_G(V_G, V_L, P_G) = [V_G] Y_{GG} V_G + [V_G] Y_{GL} V_L \\ + [I_G] R_G I_G - P_G = 0, \end{aligned} \tag{25}$$

$$f_L(V_G, V_L) = Y_{LG}\, V_G + Y_{LL}\, V_L + Y_L V_L + Y_L V_L + \bar{I}_L + [V_L]^{-1}\, \bar{P}_L = 0. \quad (26)$$

The equations (25) and (26) fundamentally depict the power balance and current balance at DGU and load nodes, respectively. These equations depend on the topology-dependent Y matrix, and are updated once a new set of decision variable is received.

In order to translate the power references into suitable voltage references, the secondary layer solves an optimization problem, whose objective is to minimize the difference between the reference power $\bar{P}_G$ and the DGU input power P_G under the equilibrium relations (25) and (26). We first consider the following simplified version of the optimization problem, where nodal voltages and generator power are not bounded.

Secondary Power Flow (SPF):

$$J_{SPF}(\bar{P}_G, \bar{P}_L, \bar{I}_L) = \min_{V_G, V_L, P_G} \; ||P_G - \bar{P}_G||_2 \quad (27a)$$

subject to

$$f_G(V_G, V_L, P_G) = 0 \quad (27b)$$

$$f_L(V_G, V_L) = 0 \quad (27c)$$

As noticeable from Figure 2, the SPF layer requires the updated load consumption $(\bar{P}_L, \bar{I}_L)$ and the power references $\bar{P}_G$ in order to solve (27). We define $\mathcal{X}$ to be the set of all (V_G, V_L, P_G) that satisfy (27b)-(27c) simultaneously. Hereafter, we will discuss necessary and sufficient conditions ensuring that the set $\mathcal{X}$ is nonempty. We start by introducing two preliminary Lemmas.

Lemma IV.1. *The matrix Y_{LL} can be written as*

$$Y_{LL} = \hat{Y}_{LL} + [-Y_{LG}\boldsymbol{I}_n], \quad (28)$$

where $\hat{Y}_{LL}$ is a Laplacian matrix .

Proof. The network admittance matrix Y is a Laplacian with zero row sum [30]. Matrix Y_{LL}, a submatrix of Y, is symmetric with positive diagonal and non-negative off-diagonal entries. Since the network graph $\mathcal{G}$ is connected, Y_{LL} has at least one row with strictly positive row sum. Y_{LL} is a Laplacian matrix with self loops [31] and, therefore, can be written as (28). □

Lemma IV.2. *The matrix $-(Y_{LL} + Y_L)^{-1}\, Y_{LG}$ has no rows with all zero entries and is nonnegative.*

Proof. The matrix $-Y_{LG}$ is a non-negative matrix and, since the graph is connected, has at least one row with non-zero row sum. The statement of the above Lemma follows from the fact that $Y_{LL} + Y_L$ is a Laplacian matrix with self loops and its inverse is strictly positive [31]. □

Next, we show that **SPF** is always feasible.

Proposition IV.1. ***(Feasibility of SPF).*** *The feasible set $\mathcal{X}$ is non-empty . In particular, for all $\bar{P}_L \in \mathbb{R}^m$ and $\bar{I}_L \in \mathbb{R}^m$, the following statements hold:*

1) The equation (27c) *is always solvable.*

2) The solvability of (27c) *implies that* (27b) *is solvable.*

Proof. Under Assumption IV.1, the equation (27c) can be written as follows:

$$[V_L]\, \tilde{Y}_{LL}\, V_L + [V_L]\, Y_{LG}\, V_G + [V_L]\, \bar{I}_L + \bar{P}_L = 0, \quad (29)$$

where $\tilde{Y}_{LL} = Y_{LL} + Y_L$. Using Banach fixed-point theorem, as shown in [25], it can be proven that for a fixed V_G, a corresponding V_L solving (27c) exists if

$$\Delta = ||P_{crit}^{-1}\, \bar{P}_L||_\infty \; < \; 1 \quad (30)$$

where

$$P_{crit} = \frac{1}{4}\, [\tilde{V}]\, \tilde{Y}_{LL}\, [\tilde{V}] \quad (31)$$

and

$$\tilde{V} = -\tilde{Y}_{LL}^{-1}\, Y_{LG} V_G - \tilde{Y}_{LL}^{-1}\, \bar{I}_L. \quad (32)$$

Different from [25], here V_G is a free variable. Therefore, for the solvability of (27c), it is enough to show that a V_G can be always found such that (30) is satisfied for any $\bar{I}_L$ and $\bar{P}_L$. Consider $V_G^\alpha = \alpha\, \mathbf{1}_n$, with $\alpha \in \mathbb{R}_{>0}$. Therefore,

$$\tilde{V}^\alpha = -\tilde{Y}_{LL}^{-1}\, Y_{LG} V_G^\alpha - \tilde{Y}_{LL}^{-1}\, \bar{I}_L = \alpha(-\tilde{Y}_{LL}^{-1}\, Y_{LG}\mathbf{1}_n) - \tilde{Y}_{LL}^{-1}\, \bar{I}_L.$$

Given Lemma IV.2, $(-\tilde{Y}_{LL}^{-1}\, Y_{LG}\mathbf{1}_n)$ is a positive vector. Hence, there exists an $\bar{\alpha} \in \mathbb{R}_{>0}$ such that $\tilde{V}^\alpha > 0 \quad \forall \alpha > \bar{\alpha}$.

Considering $i, j \in \mathcal{L}$, any element (i, j) of the matrix $(P_{crit}^\alpha)^{-1}$ can be expressed as follows

$$(P_{crit}^\alpha)_{ij}^{-1} \; = \; 4\, (\tilde{Y}_{LL})_{i,j}^{-1} / (\tilde{V}_i^\alpha \; \tilde{V}_j^\alpha). \quad (33)$$

It is evident that $(P_{crit}^\alpha)_{ij}^{-1}$ is inversely proportional to the parameter α, for $\alpha > \bar{\alpha}$. As a result, it is always possible to increase α such that (30) is verified for any $\bar{P}_L$ and $\bar{I}_L$. Consequently, a voltage solution (V_G^*, V_L^*) of (27c) always exists, proving statement 1.
Regarding statement 2, it is evident that (27b) is linear with respect to P_G. This implies that, for any solution (V_G^*, V_L^*) of (27c), a corresponding P_G^* solving (27b) always exists. □

Proposition IV.1 guarantees the feasibility of **SPF**. We now discuss optimality. If **SPF** achieves the optimal cost $J_{SPF}^* = 0$, it implies that a voltage solution exists such that the power references $\bar{P}_G$ are exactly tracked by the DGUs. This condition can not be achieved for any value of $(\bar{P}_L, \bar{I}_L, \bar{P}_G)$. The following proposition, inspired by [32], presents a necessary condition that must hold for $J_{SPF}^* = 0$. The proof nonetheless is different as here DGU filter losses are also taken into account.

Proposition IV.2. *If the **SPF** achieves the optimal cost $J_{SPF}^* = 0$, then*

$$\sum_{\forall i \in \mathcal{D}} \bar{P}_G \geq \sum_{\forall i \in \mathcal{L}} \bar{P}_L - \frac{1}{4}\, \bar{I}_L^T\, \tilde{Y}_{GG}^{-1}\, \bar{I}_L, \quad (34)$$

where $\tilde{Y}_{GG} = Y_{GG} \; - \; Y_{GL}^T (Y_{LL} + Y_L) Y_{GL}$.

Proof. Under Assumption 1, equations (27b) and (27c) can be expressed in a single matrix equality as follows

$$f(V,P_G) = [V]\,\tilde{Y}\,V \;+\; [V]\widetilde{I} \;+\; \begin{bmatrix} [I_G]\,R\,I_G \\ \mathbf{0} \end{bmatrix} + \begin{bmatrix} -P_G \\ \bar{P}_L \end{bmatrix} = \mathbf{0}_{n+m}, \tag{35}$$

where $\widetilde{I} = \begin{bmatrix}\mathbf{0}_n^T & I_L^T\end{bmatrix}^T$, and $\tilde{Y} = Y + \begin{bmatrix}\mathbf{0} & \mathbf{0} \\ \mathbf{0} & Y_L\end{bmatrix}$. To achieve $J^*_{SPF} = 0$, a solution (V, P_G) to **SPF** must exist such that $P_G = \bar{P}_G$ and

$$f(V,\bar{P}_G) = \mathbf{0}_{n+m}. \tag{36}$$

On multiplying the above equation by $\mathbf{1}^T_{n+m}$ on both sides, one obtains

$$\mathbf{1}^T_{n+m}\, f(V,\bar{P}_G) = V^T\,\tilde{Y}\,V \;+\; V^T\,\widetilde{I} \;+\; I_G^T\,R\,I_G - \mathbf{1}_n^T\,P_G \;+\; \mathbf{1}_m^T\,\bar{P}_L \;=\; 0\,. \tag{37}$$

If the solution exists for (35), then, one can also verify (36). Using simple computations, equation (37) can be rewritten as

$$(V + \frac{1}{2}\tilde{Y}^{-1}\widetilde{I})^T\,\tilde{Y}\,(V + \frac{1}{2}\tilde{Y}^{-1}\widetilde{I}) + I_G^T\,R_G\,I_G \;=\; \frac{1}{4}\,\widetilde{I}^T\,\tilde{Y}^{-1}\,\widetilde{I} + \sum_{\forall i\in\mathcal{D}} \bar{P}_G \;-\; \sum_{\forall i\in\mathcal{L}} \bar{P}_L. \tag{38}$$

Note that the matrices $\tilde{Y} \succ 0$ and $R_G \succ 0$, and hence, if a voltage solution V exists, then

$$(V + \frac{1}{2}\tilde{Y}^{-1}\widetilde{I})^T\,\tilde{Y}\,(V + \frac{1}{2}\tilde{Y}^{-1}\widetilde{I}) + I_G^T\,R\,I_G \;\geq 0. \tag{39}$$

We highlight that I_G is a function of V (see (23a)). This further implies that

$$\frac{1}{4}\,\widetilde{I}^{\,T}\,\tilde{Y}^{-1}\,\widetilde{I} + \sum_{\forall i\in\mathcal{D}} \bar{P}_G \;-\; \sum_{\forall i\in\mathcal{L}} \bar{P}_L \geq 0. \tag{40}$$

Using standard results on the inverse of block matrices, the expression $\widetilde{I}^{\,T}\,\tilde{Y}^{-1}\,\widetilde{I}$ can be simplified as $\bar{I}_L^{\,T}\,(\,\tilde{Y}_{GG}\,)^{-1}\,\bar{I}_L$, where $\tilde{Y}_{GG}$ is the Schur complement of $\tilde{Y}$ [33]. □

Remark IV.2. *It is highlighted that the necessary condition* (34) *depends only on the network parameters and load consumption. Therefore, it can be incorporated in the EMS optimization problem as a constraint for the choice of the power references $\bar{P}_G$.*

In a real DCmG, the power output P_G is constrained by physical limits of the DGUs. Moreover, the components of the DCmG are designed to operate around the nominal voltage. Hence, both nodal voltages and DGU powers must respect certain bounds, which are not incorporated in the aforementioned **SPF**. Consequently, we now introduce the following constrained optimization problem with additional operational constraints.

Secondary Constrained Power Flow (SCPF):

$$J_{SCPF}(\bar{P}_G,\bar{P}_L,\bar{I}_L) \;=\; \min_{V_G,\,V_L,P_G} \;||P_G - \bar{P}_G||_2 \tag{41a}$$

subject to

$$f_G(V_G,V_L,P_G) = 0 \tag{41b}$$
$$f_L(V_G,V_L) = 0 \tag{41c}$$
$$V_G^{min} \leq V_G \leq V_G^{max} \tag{41d}$$
$$V_L^{min} \leq V_L \leq V_L^{max} \tag{41e}$$
$$P_G^{min} \leq P_G \leq P_G^{max} \tag{41f}$$

The feasibility of **SPF**, corresponding to solving (41a)-(41c), is already ensured by Proposition IV.1. Considering the voltages and power bounds (41d)-(41f), the overall feasibility of **SCPF** is not a priori guaranteed. Nevertheless, if the DCmG is properly designed, a feasible solution of **SCPF** should always exist. In fact, the infeasibility of the **SCPF** just implies the absence of sufficient power generation to satisfy the load demand and losses in the allowed voltage range.

Next we study the properties of an optimal solution $\mathbf{x}^* = (V_G^*, V_L^*, P_G^*)$ of **SCPF**, assuming it exists. As mentioned before, the secondary control layer acts as an interface between the EMS (tertiary layer) and the local voltage regulators (primary layer). The voltage V_G^* obtained from the **SCPF** is transmitted as a reference to the primary voltage controllers of the DGUs. We highlight that just the component V_G^* of $\mathbf{x}^*$ can be directly imposed, since the load nodes are not equipped with voltage controllers and the generators are not controlled to track power references. Therefore, it is important to guarantee that, for a given voltage reference V_G^* at DGU nodes, P_G^* is the power effectively produced and V_L^* appears at the load nodes. This implies that for a fixed V_G^*, the unique solution satisfying the power flow equation (25)-(26) must be $V_L = V_L^*$, $P_G = P_G^*$. We show the uniqueness by means of the following theorem.

Theorem IV.1. ***(Uniqueness of a voltage solution).*** *Consider the solution $\boldsymbol{x}^* = (V_G^*, V_L^*, P_G^*)$ from the **SCPF** optimization problem. For a fixed V_G^*, the pair (V_L^*, P_G^*) is the unique solution of* (25)-(26) *in the set $\mathcal{Y} = \{(V_L, P_G) : V_L > V_L^{min},\ P_G \in \mathbb{R}^n\}$ if*

$$\bar{P}_{L,i} < (V_i^{min})^2\,Y_{L,i}, \quad \forall i \in \tilde{\mathcal{L}}. \tag{42}$$

Proof. For a fixed V_G^*, the power-flow equations (25)-(26) can be rewritten as

$$\tilde{f}_G(V_L,P_G) = \left.f_G(V_G,V_L,P_G)\right|_{V_G=V_G^*} = [V_G^*]Y_{GG}V_G^* + [V_L]Y_{LG}V_L + [I_G]R_GI_G - P_G = 0, \tag{43}$$

$$\tilde{f}_L(V_L) = \left.f_L(V_G,V_L)\right|_{V_G=V_G^*} = Y_{LG}\,V_G^* + Y_{LL}\,V_L + Y_LV_L + \bar{I}_L + [V_L]^{-1}\,\bar{P}_L = 0. \tag{44}$$

We will proceed by analyzing equation (44). Note that $\tilde{f}(V_L^*) = 0$ since V_L^* is a feasible solution obtained from the **SCPF**. Moreover, if the function $\tilde{f}_L(V_L)$ is injective, then V_L^* is the unique solution of (44).

To show the injectivity of $\tilde{f}_L(V_L)$, we first evaluate its Jacobian with respect to V_L, given as

$$\mathcal{J}(V_L) = \frac{\partial \tilde{f}_L(V_L)}{\partial V_L} = Y_{LL} + Y_L - \left[[V_L]^{-2}\bar{P}_L\right]. \quad (45)$$

As stated in [34, Theorem 6], if the Jacobian (45) of the function $\tilde{f}_L(V_L)$ is symmetric and positive definite in a convex region Ω, then $\tilde{f}_L(V_L)$ is injective in Ω. Note that $\mathcal{J}(V_L)$ is symmetric by construction. Moreover, using Lemma IV.1, one can split (45) into

$$\mathcal{J}(V_L) = \hat{Y}_{LL} + \underbrace{\left[-Y_{LG}\mathbf{1}_n\right] + Y_L - \left[[V_L]^{-2}\bar{P}_L\right]}_{\tilde{M}}, \quad (46)$$

where $\hat{Y}_{LL} \succeq 0$ and $-Y_{LG}$ is a nonnegative matrix. For $\mathcal{J}(V_L)$ to be positive definite, it is sufficient to show that $\tilde{M} \succ 0$. Since $\tilde{M}$ is a diagonal matrix,

$$-\sum_{j\in\mathcal{D}} Y_{ij} + Y_{L,i} - \bar{P}_{L,i}V_i^{-2} > 0, \quad \forall i \in \tilde{\mathcal{L}}. \quad (47)$$

We remark that $-\sum_{j\in\mathcal{D}} Y_{ij}$ is positive only if load i is connected directly to at least one DGU, and is otherwise zero. Hence, if

$$\bar{P}_{L,i} < V_i^2\, Y_{L,i}, \quad (48)$$

then (47) is automatically satisfied and consequently $\mathcal{J}(V_L) \succ 0$. Using (48), one can deduce that $\tilde{f}_L(V_L)$ is injective in Ω given as

$$\Omega = \{\, V_i :\ V_i > \sqrt{\frac{\bar{P}_{L,i}}{Y_{L,i}}}, \quad \forall i \in \tilde{\mathcal{L}}\,\}.$$

Since $V_{Li}^* \in [\,V_{Li}^{min}, V_{Li}^{max}\,]$ and (42) holds, V_L^* always belongs to Ω. The uniqueness of V_L^* in Ω follows from the injectivity of $\tilde{f}_L(V_L)$; moreover, given (42), V_L^* is unique in $\mathcal{Y}$. Consequently, considering that $\tilde{f}_G(V_L^*, P_G^*) = 0$, it is evident that $P_G = P_G^*$ is the unique solution of (43) if $V_G = V_G^*$ and $V_L = V_L^*$. □

Remark IV.3. ***(Condition*** (42) ***and stability).*** *The uniqueness condition* (42) *essentially limits the power consumption of P loads. As shown in [9], due to the negative impedance introduced by the P loads, their power consumption $P_{L,i} < (V_i^*)^2 Y_{L,i}, i \in \tilde{\mathcal{L}}$ in order to guarantee stability. Since V_i^* is the solution of **SCPF**, $V_i^* \geq V_i^{min}$, by satisfying* (42)*, one can simultaneously guarantee the uniqueness of load voltages and the stability of the DCmG.*

Remark IV.4. *The use of a multi-layered hierarchical control scheme is a well-established concept for the overall operation of a mG [6]. In the context of islanded DCmGs, supervisory control structures with different functionalities are explored in [3], [15], [16], [21]. However, these contributions are restricted to a specific topology, do not consider the interface with the primary layer, or disregard the stability of the DCmG. Besides the incorporation of generic topologies changing over time and the seamless integration of multiple control layers, this work considers both overall mG stability and optimal resource allocation at the same time. Moreover, the secondary control layer can easily be interfaced with any EMS that generates power references.*

V. Numerical Results

In this section, we aim to show the performance of the proposed hierarchical control scheme via simulation studies conducted in MATLAB. We consider the 16-bus DC feeder in meshed stand-alone configuration described in [1], equipped with three battery DGUs, two dispatchable DGUs, a PV DGU, and ten ZIP loads (see Figure 3). The DGUs are interfaced with synchronous Buck converters and controlled by the primary voltage controllers studied in [9]. We highlight that turning off dispatchable DGUs at nodes 1 and 2 simultaneously splits the mG into two separate DCmGs (see Figure 3), and can be circumvented by adding the simple constraint $\delta_{D,1}(k+i)+\delta_{D,2}(k+i) \geq 1, \forall i \in [0,\ldots,N-1]$, to the EMS optimization problem (21). The loads are standard ZIP, and their power and current absorption follow three different daily profiles denoted by subscripts a, b, and c (depicted in Figure 4). The DCmG is operated at a nominal voltage $V^o = 100$ Volts with nodal voltages lying between $V^{min} = 0.9V^o$ and $V^{max} = 1.1V^o$. The DGU parameters utilized by the EMS are given in Table II.

The MPC-based EMS schedules the optimal power setpoints of DGUs every 15 minutes, using a prediction horizon of 5 hours, i.e. $N = 20$. The secondary layer runs with a sampling time of 3 minutes with the goal of tracking the received power references despite the aforementioned load variations.

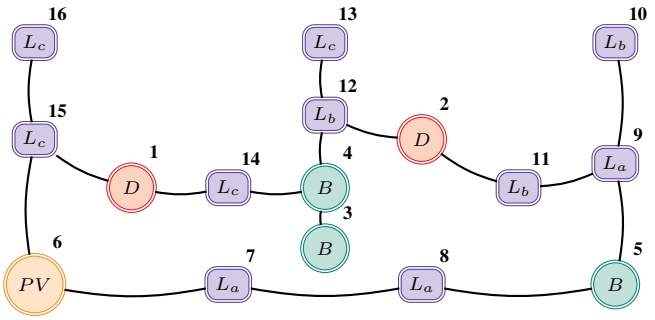

Fig. 3: DCmG based on the modified 16-bus feeder [1]. The letters D, B, and PV denote dispatchable, battery, and PV DGUs, respectively. The letter L indicates loads with subscripts a, b, and c defining different consumption patterns.

DGU	$(P^{min},\ P^{max})$	(η_{CH}, η_{DH})	$(S_B^{min},\ S_B^{max})$	S_B^o
D1	$(+10, +80)$	–	–	–
D2	$(+10, +80)$	–	–	–
B3	$(-40, +40)$	(0.9, 0.9)	(0.1, 0.9)	0.5
B4	$(-50, +50)$	(0.9, 0.9)	(0.1, 0.9)	0.6
B5	$(-60, +60)$	(0.9, 0.9)	(0.1, 0.9)	0.4

TABLE II: DGU parameters used by the EMS.

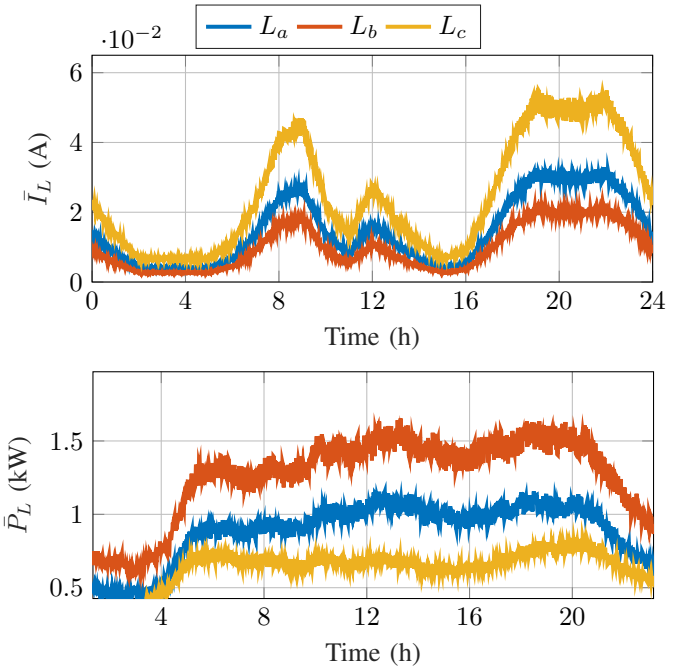

Fig. 4: Actual current and power absorption of DCmG loads. Each of the 10 DCmG loads corresponds to one of the three profiles shown above.

In the ensuing discussion, we describe the behaviour of various mG components controlled by the proposed hierarchical controller over a span of 24 hours.

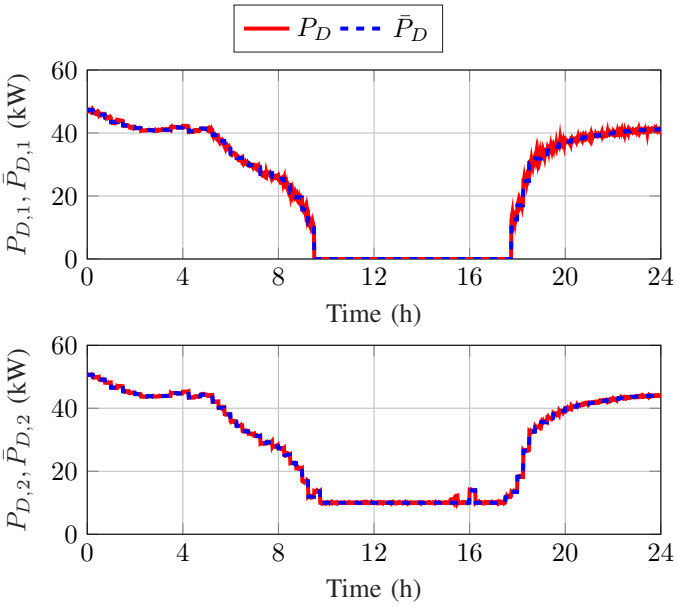

Fig. 5: Power generated by dispatchable DGUs).

Dispatchable DGUs: As shown in Figure 5, DGUs D1 and D2 track the power references provided by the EMS. During the day, when PV generation starts picking up (see Figure 8), the EMS turns off DGU D1 to ensure economic optimality and maintain mG power balance. DGU D2, although producing minimum permissible power during the period of peak PV generation, remains operational throughout the day in order to maintain connectivity of the DCmG.

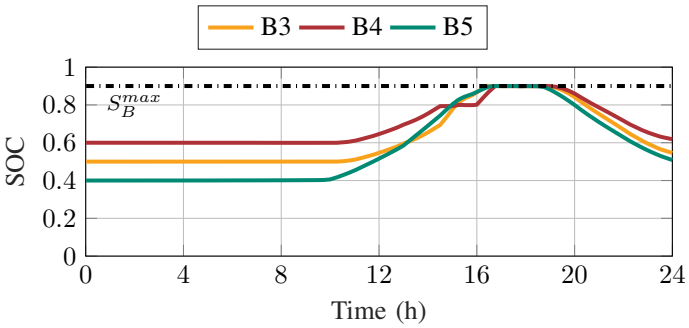

Fig. 6: States of charge of DGUs B3, B4, and B5.

Battery DGUs: In Figure 7, it can be noticed that battery DGUs follow power references provided by the EMS. Abrupt charging and discharging, and frequent switching between these two modes work to the detriment of battery's longevity, and are prevented by the EMS. As for the SOCs, reported in Figure 6, they evolve respecting the operational constraints. Moreover, the EMS tries to store surplus energy during periods of peak PV generation (see Figure 8). This energy is released in the last part of the day during which the PV generation declines.

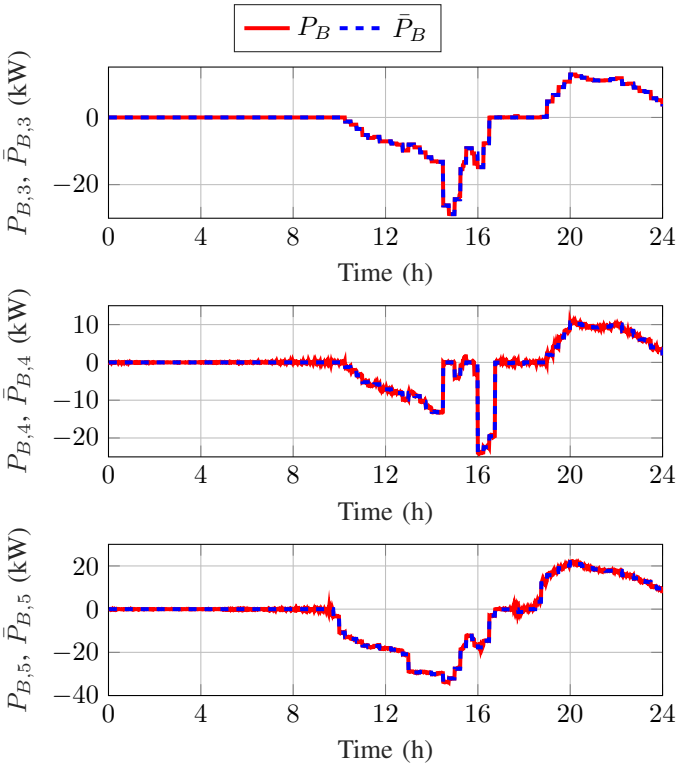

Fig. 7: Power output by battery DGUs.

PV DGU: As reported in Figure 8, so as to be consistent with a real operation scenario, the simulations have been conducted with a mismatch between nominal PV generation and forecasts. At each sampling instant, the EMS utilizes the nominal PV generation and the forecast not only to generate

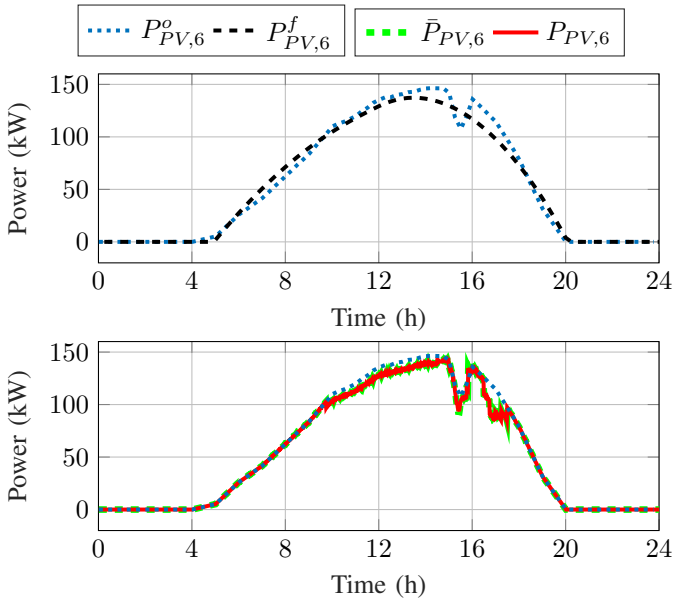

Fig. 8: Nominal generation, PV generation forecast, EMS power reference, generated power for DGU PV6.

power references but also to decide whether to operate the PV DGU in MPPT or power curtailment mode. As seen from Figure 8, the power injected by the PV generators into the DCmG tracks the EMS power references. Notice that the PV DGU operates in MPPT mode during the first and the last hours of the simulation, whereas it curtails power during the central part of the day. Clearly, a power curtailment is inevitable considering that the SOCs are going to hit their upper bound, DGU D1 is nonoperational, while DGU D2 is injecting minimum power and it cannot be switched off.

Loads: The load power forecasts used by the EMS and the net power absorption for nodes 8, 11, and 16 are shown in Figure 9. One can observe that the forecasts are fairly different from the actual power absorption. This stems from the fact that EMS forecasts are deduced using inaccurate current and power profiles (see Figure 4 for actual current and power absorption) at nominal voltage. Even if exact profiles were available to the EMS *a priori*, the forecasts would not coincide with net power absorbed by the loads. This is because the net power absorbed by a load depends on PCC voltage, which is generated by the secondary layer only after EMS power references are received.

Finally, we highlight that, during the simulation, the condition (42) always holds for all load nodes, ensuring the uniqueness of solution for load voltages and the perfect tracking of DGUs power injections. The secondary control layer manipulates the voltage references of the DGUs every 3 minutes, and maintains the voltages in the allowed range, as shown in Figure 10. As a consequence of new power references received from the EMS, a clear change in voltages can be observed every 15 minutes. In Figure 11, we show the performance of primary voltage controllers when dispatchable DGU D1 is turned off by the EMS. Indeed, thanks to the implemented Plug-n-Play controllers, the transients quickly die out and voltages are forced back to desired reference values.

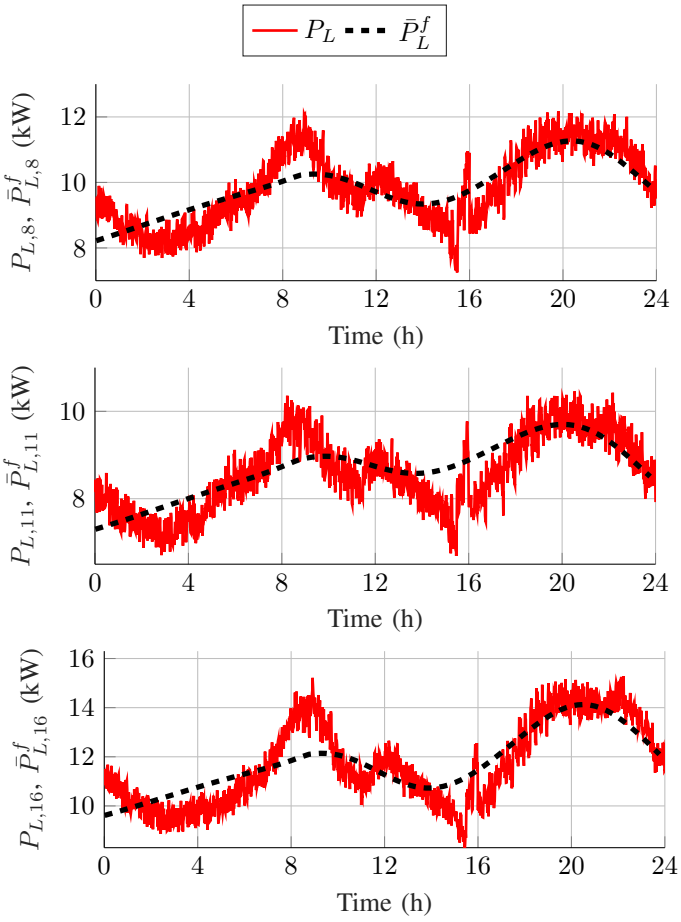

Fig. 9: Load power forecasts and net power absorption for different load nodes.

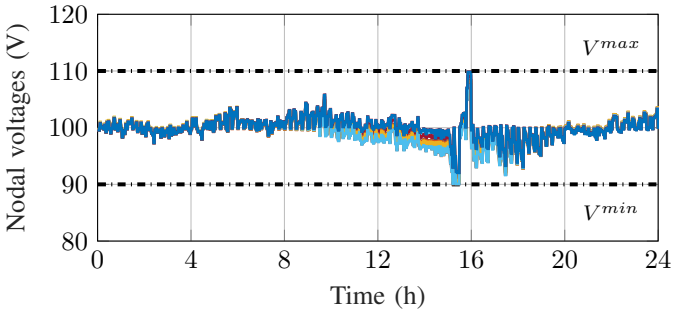

Fig. 10: Nodal voltages in the DCmG network.

VI. Conclusions

In this work, we proposed a top-to-bottom hierarchical control structure for an islanded DCmG. Our supervisory controller resting atop a primary voltage layer comprises secondary and tertiary layers. By utilizing an MPC-based EMS at tertiary layer, optimal power references are generated. The secondary layer translates these power signals into voltage references for the primary layer. More specifically, the voltage references are generated by solving an optimization problem at the secondary layer, which can incorporate practical operational constraints. Furthermore, we studied the well-possessedness of the secondary optimization problem by

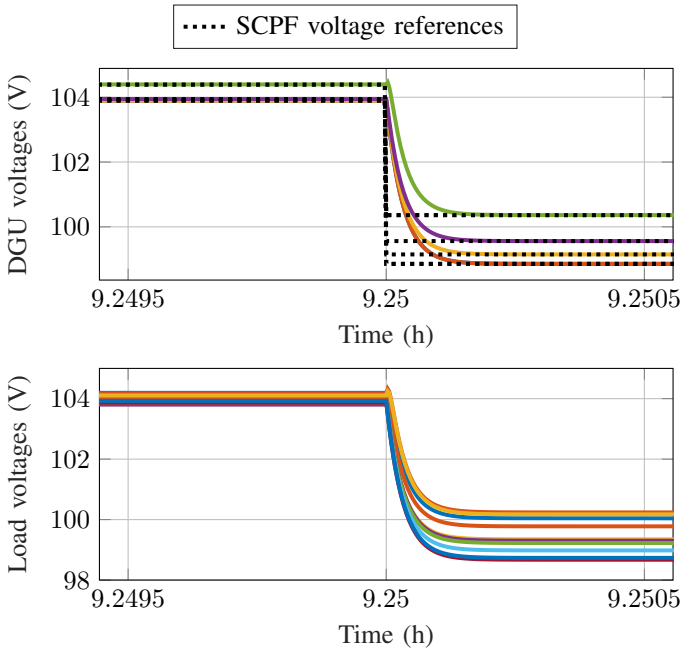

Fig. 11: Nodal voltages when dispatchable DGU D1 is turned off.

discussing its feasibility and deduced a novel condition for the uniqueness of generator voltages and DGU power injections. Lastly, we demonstrated multiple layers of our hierarchical controller working in tandem to achieve desired objectives on a 16-node mG. Future work will target the development of an EMS that enables the mG to work in grid-connected mode, and a secondary control layer that does away with the dependence on mG topology. Further developments can also focus on solving the proposed optimization problem in a distributed and efficient manner.

REFERENCES

[1] J. Li, F. Liu, Z. Wang, S. H. Low, and S. Mei, "Optimal power flow in stand-alone DC microgrids," *IEEE Transactions on Power Systems*, vol. 33, no. 5, pp. 5496–5506, Sep. 2018.

[2] A. La Bella, S. Negri, R. Scattolini, and E. Tironi, "A two-layer control architecture for islanded AC microgrids with storage devices," in *2018 IEEE Conference on Control Technology and Applications (CCTA)*. IEEE, 2018, pp. 1421–1426.

[3] Q. Shafiee, J. M. Guerrero, and J. C. Vasquez, "Distributed Secondary Control for Islanded Microgrids : A Novel Approach," *IEEE Transactions on Power Electronics*, vol. 29, no. 2, pp. 1018–1031, 2014.

[4] M. Babazadeh and H. Karimi, "A robust two-degree-of-freedom control strategy for an islanded microgrid," *IEEE Transactions on power delivery*, vol. 28, no. 3, pp. 1339–1347, 2013.

[5] T. Dragičević, X. Lu, J. C. Vasquez, and J. M. Guerrero, "DC microgrids part I: A review of control strategies and stabilization techniques," *IEEE Transactions on Power Electronics*, vol. 31, no. 5, pp. 4876–4891, 2016.

[6] L. Meng, Q. Shafiee, G. Ferrari-Trecate, H. Karimi, D. Fulwani, X. Lu, and J. M. Guerrero, "Review on control of DC microgrids and multiple microgrid clusters," *IEEE Journal of Emerging and Selected Topics in Power Electronics*, vol. 5, no. 3, pp. 928–948, 2017.

[7] A. Bidram and A. Davoudi, "Hierarchical structure of microgrids control system," *IEEE Transactions on Smart Grid*, vol. 3, no. 4, pp. 1963–1976, Dec 2012.

[8] A. La Bella, S. R. Cominesi, C. Sandroni, and R. Scattolini, "Hierarchical predictive control of microgrids in islanded operation," *IEEE Transactions on Automation Science and Engineering*, vol. 14, no. 2, pp. 536–546, 2017.

[9] P. Nahata, R. Soloperto, M. Tucci, A. Martinelli, and G. Ferrari-Trecate, "A passivity-based approach to voltage stabilization in islanded DC microgrids with ZIP loads," Tech. Rep., 2017. [Online]. Available: https://infoscience.epfl.ch/record/253266?ln=en

[10] A. Martinelli, P. Nahata, and G. Ferrari-Trecate, "Voltage stabilization in MVDC microgrids using passivity-based nonlinear control," in *2018 IEEE Conference on Decision and Control (CDC)*, Dec 2018, pp. 7022–7027.

[11] M. Cucuzzella, S. Rosti, A. Cavallo, and A. Ferrara, "Decentralized sliding mode voltage control in dc microgrids," in *2017 American Control Conference (ACC)*. IEEE, 2017, pp. 3445–3450.

[12] M. Tucci, L. Meng, J. M. Guerrero, and G. Ferrari-Trecate, "Stable current sharing and voltage balancing in dc microgrids: A consensus-based secondary control layer," *Automatica*, vol. 95, pp. 1 – 13, 2018.

[13] P. Nahata and G. Ferrari-Trecate, "On existence of equilibria, voltage balancing, and current sharing in consensus-based DC microgrids," in *19th European Control Conference (ECC)*, 2020, submitted.

[14] A. Martinelli, A. La Bella, and R. Scattolini, "Secondary control strategies for dc islanded microgrids operation," in *2019 18th European Control Conference (ECC)*. IEEE, 2019, pp. 897–902.

[15] M. Kumar, S. C. Srivastava, and S. N. Singh, "Control strategies of a DC microgrid for grid connected and islanded operations," *IEEE Transactions on Smart Grid*, vol. 6, no. 4, pp. 1588–1601, July 2015.

[16] T. Dragičević, J. M. Guerrero, and J. C. Vasquez, "Supervisory control of an adaptive-droop regulated dc microgrid with battery management capability," *IEEE Transactions on Power Electronics*, vol. 29, no. 2, pp. 695–706, Feb 2014.

[17] M. Marzband, F. Azarinejadian, M. Savaghebi, and J. M. Guerrero, "An optimal energy management system for islanded microgrids based on multiperiod artificial bee colony combined with markov chain," *IEEE Systems Journal*, vol. 11, no. 3, pp. 1712–1722, 2017.

[18] C. A. Hans, P. Sopasakis, A. Bemporad, J. Raisch, and C. Reincke-Collon, "Scenario-based model predictive operation control of islanded microgrids," in *2015 54th IEEE Conference on Decision and Control (CDC)*, Dec 2015, pp. 3272–3277.

[19] A. Parisio, E. Rikos, and L. Glielmo, "Stochastic model predictive control for economic/environmental operation management of microgrids: An experimental case study," *Journal of Process Control*, vol. 43, pp. 24–37, 2016.

[20] S. R. Cominesi, A. La Bella, M. Farina, and R. Scattolini, "A multi-layer control scheme for microgrid energy management," *IFAC-PapersOnLine*, vol. 49, no. 27, pp. 256–261, 2016.

[21] A. Iovine, T. Rigaut, G. Damm, E. De Santis, and M. D. Di Benedetto, "Power management for a dc microgrid integrating renewables and storages," *Control Engineering Practice*, vol. 85, pp. 59–79, 2019.

[22] A. S. Matveev, J. E. Machado, R. Ortega, J. Schiffer, and A. Pyrkin, "On the existence and long-term stability of voltage equilibria in power systems with constant power loads," *arXiv preprint arXiv:1809.08127*, 2018.

[23] R. Han, M. Tucci, A. Martinelli, J. M. Guerrero, and G. Ferrari-Trecate, "Stability analysis of primary plug-and-play and secondary leader-based controllers for DC microgrid clusters," *IEEE Transactions on Power Systems*, vol. 34, no. 3, pp. 1780–1800, May 2019.

[24] M. Tucci, S. Riverso, and G. Ferrari-Trecate, "Line-independent plug-and-play controllers for voltage stabilization in dc microgrids," *IEEE Transactions on Control Systems Technology*, vol. 26, no. 3, pp. 1115–1123, May 2018.

[25] J. W. Simpson-Porco, F. Dörfler, and F. Bullo, "Voltage collapse in complex power grids," *Nature communications*, vol. 7, p. 10790, 2016.

[26] S. Taheri and V. Kekatos, "Power flow solvers for direct current networks," *arXiv preprint arXiv:1807.03936*, 2018.

[27] A. La Bella, P. Nahata, and G. Ferrari-Trecate, "A supervisory control structure for voltage-controlled islanded DC microgrids," in *58th IEEE Conference on Decision and Control*, 2019.

[28] P. Kundur, *Power System Stability and Control*. McGraw-Hill, 1994.

[29] A. Bemporad and M. Morari, "Control of systems integrating logic, dynamics, and constraints," *Automatica*, vol. 35, no. 3, pp. 407 – 427, 1999.

[30] F. Dörfler, J. W. Simpson-Porco, and F. Bullo, "Electrical networks and algebraic graph theory: Models, properties, and applications," *Proceedings of the IEEE*, vol. 106, no. 5, pp. 977–1005, 2018.

[31] F. Dörfler and F. Bullo, "Kron reduction of graphs with applications to electrical networks," *IEEE Transactions on Circuits and Systems I: Regular Papers*, vol. 60, no. 1, pp. 150–163, 2013.

[32] S. Sanchez, R. Ortega, R. Grino, G. Bergna, and M. Molinas, "Conditions for existence of equilibria of systems with constant power loads,"

IEEE Transactions on Circuits and Systems I: Regular Papers, vol. 61, no. 7, pp. 2204–2211, 2014.

[33] T.-T. Lu and S.-H. Shiou, "Inverses of 2 by 2 block matrices," *Computers and Mathematics with Applications*, vol. 43, no. 1, pp. 119 – 129, 2002.

[34] D. Gale and H. Nikaido, "The Jacobian matrix and global univalence of mappings," *Mathematische Annalen*, vol. 159, no. 2, pp. 81–93, 1965.